Biogenesis of sperm acrosome is regulated by pre-mRNA alternative splicing of *Acrbp* in the mouse

Yoshinori Kanemori[a,b], Yoshitaka Koga[a], Mai Sudo[a], Woojin Kang[a,1], Shin-ichi Kashiwabara[a,b], Masahito Ikawa[c], Hidetoshi Hasuwa[c,2], Kiyoshi Nagashima[a,b], Yu Ishikawa[a,b], Narumi Ogonuki[d], Atsuo Ogura[a,d], and Tadashi Baba[a,b,e,3]

[a]Faculty of Life and Environmental Sciences, University of Tsukuba, Tsukuba Science City, Ibaraki 305-8572, Japan; [b]PhD Program in Human Biology, School of Integrative and Global Majors, University of Tsukuba, Tsukuba Science City, Ibaraki 305-8572, Japan; [c]Research Institute for Microbial Diseases, Osaka University, Suita, Osaka 565-0871, Japan; [d]RIKEN BioResource Center, Tsukuba Science City, Ibaraki 305-0074, Japan; and [e]Life Science Center of Tsukuba Advanced Research Alliance, University of Tsukuba, Tsukuba Science City, Ibaraki 305-8577, Japan

Edited by John J. Eppig, The Jackson Laboratory, Bar Harbor, ME, and approved May 16, 2016 (received for review November 12, 2015)

Proper biogenesis of a sperm-specific organelle, the acrosome, is essential for gamete interaction. An acrosomal matrix protein, ACRBP, is known as a proacrosin-binding protein. In mice, two forms of ACRBP, wild-type ACRBP-W and variant ACRBP-V5, are generated by pre-mRNA alternative splicing of *Acrbp*. Here, we demonstrate the functional roles of these two ACRBP proteins. ACRBP-null male mice lacking both proteins showed a severely reduced fertility, because of malformation of the acrosome. Notably, ACRBP-null spermatids failed to form a large acrosomal granule, leading to the fragmented structure of the acrosome. The acrosome malformation was rescued by transgenic expression of ACRBP-V5 in ACRBP-null spermatids. Moreover, exogenously expressed ACRBP-W blocked autoactivation of proacrosin in the acrosome. Thus, ACRBP-V5 functions in the formation and configuration of the acrosomal granule during early spermiogenesis. The major function of ACRBP-W is to retain the inactive status of proacrosin in the acrosome until acrosomal exocytosis.

mouse | spermiogenesis | fertilization | acrosomal biogenesis | alternative splicing

The acrosome of mammalian sperm is a cap-shaped, exocytotic vesicle present on the apical surface of the head (1, 2). Acrosomal biogenesis takes place at the initial step of spermiogenesis, a process during which haploid spermatids differentiate into sperm and which can be divided into four phases: the Golgi, cap, acrosome, and maturation phases (1–5). In rodent spermatids, proacrosomal vesicles (granules) containing a variety of proteins assemble and fuse with one another to form a single, sphere acrosomal granule in the center of the acrosomal vesicle at the Golgi phase (1). At the cap phase, the acrosomal granule forms a head cap-like structure that gradually enlarges to cover the nucleus. The head cap continues to elongate outlining the dorsal edge, protruding apically at the acrosome phase, and then the structure of the acrosome is completed at the end of maturation phase.

The lumen of the acrosomal vesicle, which is surrounded by inner and outer acrosomal membranes, contains soluble and aggregated (acrosomal matrix) components (2, 5). The acrosome reaction is a fusion event between outer acrosomal and plasma membranes at multiple sites (2, 6). Consequently, the soluble components are dispersed from the acrosome, and the status of the sperm head is newly reorganized following gradual release of the matrix components (7). Sperm serine protease acrosin (ACR) localized in the acrosomal matrix has been shown to play a crucial role in dispersal of the acrosomal matrix components (8, 9). Because only acrosome-reacted sperm are capable of fusing with the oocyte plasma membrane, the acrosome reaction is physiologically essential for fertilization (2). Indeed, once sperm are acrosome-reacted, an acrosomal membrane-spanning protein, IZUMO1, migrates on the acrosomal membrane, is exposed on the surface of sperm head, and interacts with Juno glycosylphosphatidylinositol (GPI) anchored on the oocyte plasma membrane to achieve the sperm/oocyte fusion (10, 11).

An acrosomal protein, ACRBP (also known as sp32), is a binding protein specific for the precursor (proACR) and intermediate forms of ACR (12–14). ACRBP also has been identified as a member of the cancer/testis antigen family; *ACRBP* is normally expressed exclusively in the testis, but is also expressed in a wide range of different tumor types, including bladder, breast, liver, and lung carcinomas (15–17). Mammalian ACRBP is initially synthesized as a ∼60-kDa precursor protein (ACRBP-W) in spermatogenic cells, and the 32-kDa mature ACRBP (ACRBP-C) is posttranslationally produced by removal of the N-terminal half of the precursor ACRBP-W during spermatogenesis and/or epididymal maturation of sperm (14, 18). In the mouse, two forms of *Acrbp* mRNA, wild-type *Acrbp-W* and variant *Acrbp-V5* mRNAs, are produced by pre-mRNA alternative splicing of *Acrbp* (18). Similarly to other mammalian ACRBP-W, mouse ACRBP-W starts to be synthesized in pachytene spermatocytes and immediately processed into ACRBP-C (Fig. S1). The intron 5-retaining splice variant mRNA produces a predominant form of ACRBP, ACRBP-V5, that is also present in pachytene spermatocytes and round spermatids, but is absent in elongating spermatids (18). Functional analysis in vitro reveals that ACRBP-V5 and ACRBP-C possess a different domain capable of binding each of two segments in the C-terminal region of proACR (18). Moreover, autoactivation of proACR is remarkably accelerated by the presence of

Significance

Mammalian sperm possess a Golgi-derived exocytotic organelle, the acrosome, located on the apical region of the head. Proper biogenesis of the acrosome is essential for the fertilization process because the aberrant acrosome formation results in the sterility or subfertility of males. Here, we show that the acrosome formation is governed by two forms of proacrosin-binding protein ACRBP, wild-type ACRBP-W and variant ACRBP-V5, which are generated by pre-mRNA alternative splicing of *Acrbp*. ACRBP-V5 is involved in the formation and configuration of the acrosomal granule during early spermiogenesis, whereas the inactive status of proacrosin in the acrosome is maintained by ACRBP-W until acrosomal exocytosis.

Author contributions: Y. Kanemori and T.B. designed research; Y. Kanemori, Y. Koga, M.S., W.K., K.N., and Y.I. performed research; Y. Kanemori, Y. Koga, W.K., S.K., M.I., and H.H. generated knockout and transgenic mice; N.O. and A.O. performed intracytoplasmic sperm injection; Y. Kanemori, M.I., N.O., and T.B. analyzed data; and Y. Kanemori and T.B. wrote the paper.

The authors declare no conflict of interest.

This article is a PNAS Direct Submission.

[1]Present address: Department of Reproductive Biology, National Research Institute for Child Health and Development, Setagaya, Tokyo 157-8535, Japan.

[2]Present address: Department of Molecular Biology, Keio University School of Medicine, Shinjuku, Tokyo 160-8582, Japan.

[3]To whom correspondence should be addressed. Email: baba.tadashi.gf@u.tsukuba.ac.jp.

This article contains supporting information online at www.pnas.org/lookup/suppl/doi:10.1073/pnas.1522333113/-/DCSupplemental.

www.pnas.org/cgi/doi/10.1073/pnas.1522333113

ACRBP-C (14, 18). Thus, we postulated that, at least in the mouse, ACRBP-V5 and ACRBP-C may differentially function in the transport/packaging of proACR into the acrosomal granule during spermiogenesis and in the promotion of ACR release from the acrosome during acrosomal exocytosis, respectively.

In this study, to elucidate the physiological roles of ACRBP in spermiogenesis and fertilization, we have produced ACRBP-null mutant mice lacking both ACRBP-W and ACRBP-V5. The mutant mice were then rescued by transgenic expression of ACRBP-W or ACRBP-V5. The severely reduced fertility of ACRBP-null males was significantly recovered by introduction either of exogenous ACRBP-W or ACRBP-V5. On the basis of the data obtained, the specialized functions of ACRBP-W/ACRBP-C and ACRBP-V5 in acrosome formation and acrosomal exocytosis are discussed.

Results

Generation of Mice Lacking ACRBP. To uncover the functional role of ACRBP in spermiogenesis and fertilization, we produced mice carrying a null mutation of *Acrbp* using homologous recombination in embryonic stem (ES) cells. A targeting construct was designed to delete both ACRBP-W and the variant form ACRBP-V5 by replacing the 472-nucleotide protein-coding region of exons 1–4 with the neomycin-resistant gene *neo* (Fig. 1*A*). The genotype of wild-type ($Acrbp^{+/+}$), heterozygous ($Acrbp^{+/-}$), and homozygous ($Acrbp^{-/-}$) mice for the targeted mutation of *Acrbp* were identified by Southern blot analysis of genomic DNA (Fig. 1*B*). Immunoblot analysis of testicular protein extracts indicated the loss of 60/55- and 48/43-kDa doublets corresponding to ACRBP-W and ACRBP-V5, respectively (Fig. 1*C*). The $Acrbp^{-/-}$ testis also lacked 30-kDa ACRBP-C (14, 18) posttranslationally produced from ACRBP-W during spermatogenesis. Mating of $Acrbp^{+/-}$ male and female mice yielded an expected Mendelian frequency of $Acrbp^{-/-}$ mice [$Acrbp^{+/+}$:$Acrbp^{+/-}$:$Acrbp^{-/-}$ = 25 (21%):64 (54%):29 (25%) for 118 offspring from 10 litters] (Fig. S2*A*). $Acrbp^{-/-}$ male and female mice were normal in behavior, body size, and health condition. Although $Acrbp^{+/-}$ males exhibited normal fertility, the fertility of $Acrbp^{-/-}$ males was dramatically reduced; 3 of 10 $Acrbp^{-/-}$ males produced no offspring a month after mating with wild-type females despite normal plug formation. Even when the females that mated with the $Acrbp^{-/-}$ males became pregnant, the litter sizes were significantly decreased (Fig. 1*D*). The $Acrbp^{-/-}$ females exhibited normal fertility (Fig. S2*B*). In addition, no significant difference in the testicular weight and the number of cauda epididymal sperm were found between $Acrbp^{+/+}$ and $Acrbp^{-/-}$ (Fig. 1 *E* and *F*). These data demonstrate that the loss of ACRBP-W and ACRBP-V5 results in severely reduced male fertility.

Acrosome Formation in ACRBP-Deficient Testis. We next examined the acrosomal status of $Acrbp^{-/-}$ spermatogenic cells, using Alexa Fluor 568-conjugated peanut agglutinin (PNA) capable of binding mainly the outer acrosomal membrane (19). Consistent with already published reports (1, 20–22), a single, sphere acrosomal granule was formed in the center of the acrosomal vesicle of $Acrbp^{+/+}$ spermatids by assembly of proacrosomal vesicles at steps 2 and 3 (Golgi phase) of spermiogenesis (Fig. 2*A*). The acrosomal granule gradually enlarged to form a head cap-like structure covering the nucleus at steps 4–7 (cap phase), and then the head cap further elongated, outlining the dorsal edge. In $Acrbp^{-/-}$ spermatids, proacrosomal vesicles normally assembled at the Golgi phase. However, $Acrbp^{-/-}$ spermatids at the cap phase lacked a large acrosomal granule (arrows in Fig. 2*A*), leading to a diffuse pattern of head cap distribution in the anterior region of the nucleus (Fig. 2*B*). Consequently, the acrosomal structure of $Acrbp^{-/-}$ spermatids was severely deformed at the later steps of spermiogenesis.

To examine the localization of acrosomal proteins in $Acrbp^{-/-}$ spermatids, we carried out immunostaining analysis using antibodies against four acrosomal proteins, ACRBP-W/ACRBP-C, ACRBP-V5, proACR, and ZPBP2, and two other proteins, ZPBP1 and SPACA1, attached and anchored on the inner acrosomal membrane at the equatorial segment, respectively (Fig. 2*C*). The levels of proACR, ZPBP2, ZPBP1, and SPACA1 in testicular extracts were comparable between $Acrbp^{+/+}$ and $Acrbp^{-/-}$ mice (Fig. S3). ACRBP-W/ACRBP-C, ACRBP-V5, proACR, and ZPBP2 in $Acrbp^{+/+}$ spermatids accumulated in the acrosomal granule until steps 6 and 7 and were then distributed along the

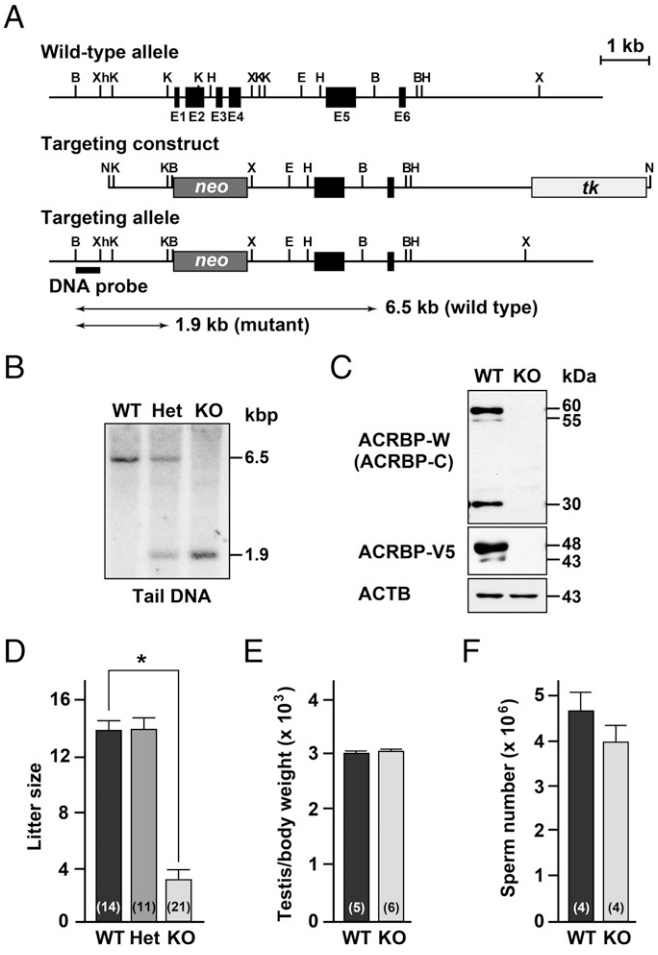

Fig. 1. Generation of ACRBP-deficient male mice. (*A*) Targeting strategy of *Acrbp*. Exons 1–4 (E1–E4, closed box) encoding the N-terminal 157-residue sequence of ACRBP (ACRBP-W and ACRBP-V5) in *Acrbp* was replaced by *neo* (darkly shaded box). For negative selection, *tk* (lightly shaded box) was included at the 3′-end of the targeting construct. Restriction enzyme sites indicated are as follows: B, BamH1; Xh, XhoI; K, KpnI; H, HindIII; X, XbaI; E, EcoRI; N, NotI. (*B*) Southern blot analysis. Genomic DNAs from wild-type ($Acrbp^{+/+}$, WT), heterozygous ($Acrbp^{+/-}$, Het), and homozygous ($Acrbp^{-/-}$, KO) mice were digested with BamHI, separated by agarose gel electrophoresis, and subjected to Southern blot analysis using a ^{32}P-labeled BamHI/XhoI fragment (DNA probe) as a probe. (*C*) Immunoblot analysis of testicular extracts. Proteins were probed with anti–ACRBP-C, anti–ACRBP-V5, and anti-ACTB (β-actin) antibodies. (*D*) Fertility of KO male mice. The WT, Het, and KO males (4, 6, and 10 different mice, respectively) were mated with WT females, and the litter sizes were counted. Total numbers of the WT females mated are indicated in parentheses. All statistical significances are calculated using the Student *t* test. $*P < 0.01$. Note that the WT and Het males examined were all fertile, and 3 of 10 KO males produced no offspring a month after mating with the females despite normal plug formation. (*E* and *F*) Testicular weight and sperm number of KO mice. The body and testis weights of WT and KO mice were measured 10–14 wk after birth (*E*). The numbers of sperm in the epididymides were also counted (*F*). The numbers in parentheses indicate those of males tested.

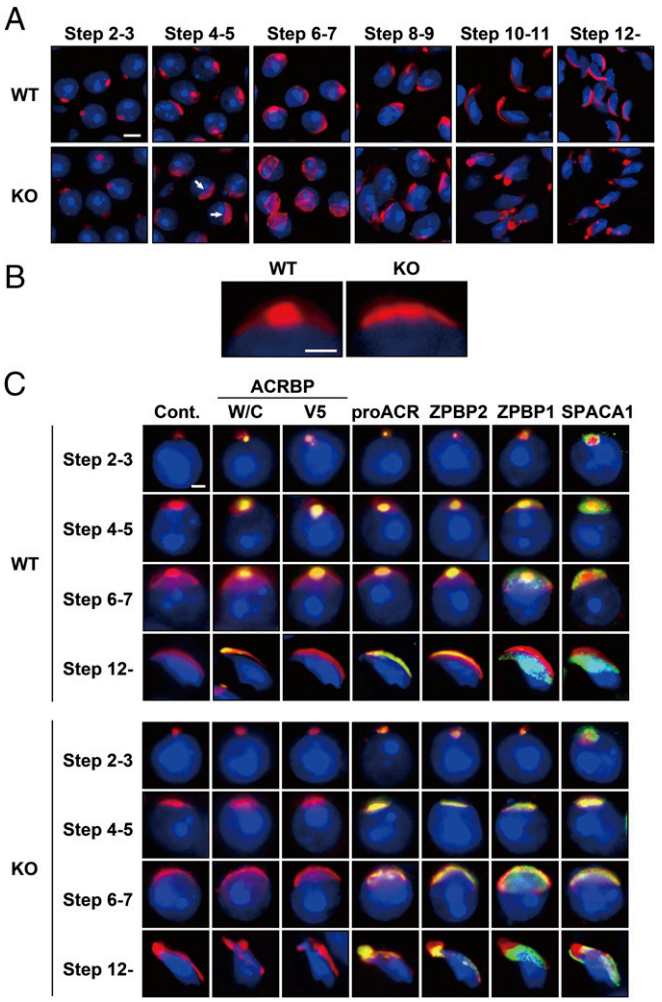

Fig. 2. Abnormal acrosomal biogenesis in ACRBP-deficient spermatids. (*A* and *B*) Absence of acrosomal granule. Haploid spermatids of wild-type (WT) and ACRBP-deficient (KO) mice were stained with fluorescent dye-labeled lectin PNA (red) and Hoechst 33342 (blue). Note that KO spermatids display a diffused pattern of head cap distribution (arrows in *A*) because of the lack of a large acrosomal granule in the center of acrosomal vesicle. (Scale bars: 6.0 and 2.0 μm in *A* and *B*, respectively. (*C*) Subcellular localization of acrosomal proteins. Spermatids were immunostained with antibodies against proteins indicated (green). The acrosome and nucleus were also stained with fluorescent dye-labeled PNA (red) and Hoechst 33342 (blue), respectively. No immunoreactive signal was detected when preimmune serum was used as the probe (Cont.). (Scale bar, 2.0 μm.)

dorsal edge of the sperm head. ZPBP1 and SPACA1 were initially present around the acrosomal granule and then spread to the equatorial region, as described previously (23, 24). Essentially similar results were obtained in $Acrbp^{+/-}$ spermatids (Fig. S4*A*). The assembly of acrosomal proteins in $Acrbp^{-/-}$ spermatids was normal at the Golgi phase (Fig. 2*C*). However, these proteins were localized throughout the acrosomal vesicle at the early cap phase, without forming an acrosomal granule-like structure, and then scattered over the nucleus, because of the fragmented structures of acrosome.

Transmission electron microscopy (TEM) images indicated no obvious difference in the morphology of spermatids at the Golgi phase between $Acrbp^{+/+}$ and $Acrbp^{-/-}$ mice (Fig. 3). The acrosomal vesicle was located adjacent to the Golgi apparatus having a well-defined polarized structure with ordered stacks of sacculi. However, $Acrbp^{-/-}$ spermatids at the cap phase displayed at least two morphological defects in the acrosome, compared with $Acrbp^{+/+}$ spermatids: the abnormal shape of the acrosomal vesicle and the lack of the electron-dense acrosomal granule in the center of acrosomal vesicle. As spermiogenesis proceeded, the morphological abnormality of the acrosome in $Acrbp^{-/-}$ spermatids became more severe. In addition to the acrosome, the nucleus of $Acrbp^{-/-}$ spermatids was deformed to some extent (Fig. 3 and Fig. S5). These results suggest that either ACRBP-W or ACRBP-V5 or both may play essential roles in the formation of the sphere acrosomal granule and in the retention of acrosomal proteins in the acrosomal granule.

Characterization of ACRBP-Deficient Epididymal Sperm. Because $Acrbp^{-/-}$ male mice exhibited a severely reduced fertility (Fig. 1*D*), we asked whether cauda epididymal sperm of $Acrbp^{-/-}$ mice are morphologically and functionally normal. Although the hook-shaped acrosome in $Acrbp^{+/+}$ sperm was also observed in $Acrbp^{+/-}$ sperm (Fig. S4*B*), $Acrbp^{-/-}$ sperm exhibited a continuous variation in the shapes of the acrosome and nucleus (Fig. 4*A*). We thus divided the whole population of $Acrbp^{-/-}$ sperm into four types (types 1, 2, 3, and 4). The nucleus of type 1 $Acrbp^{-/-}$ sperm was morphologically similar to that of $Acrbp^{+/+}$ sperm, despite the fact that the acrosome of type 1 sperm was partially fragmented on the head or was not fully elongated to the dorsal edge. The nuclear shapes of type 2 and type 3 sperm were moderately and severely affected, respectively, in addition to the fragmented structure of acrosome. Moreover, type 4 sperm displayed both the fragmented acrosome and a round-headed shape with a coiled midpiece around the deformed nucleus, similarly to GOPC-, ZPBP1-, and SPACA1-null sperm (23–25). The rates of type 1, type 2, type 3, and type 4 sperm were ~50%, 34%, 12%, and 4% of total $Acrbp^{-/-}$ sperm, respectively. The morphological change may occur during sperm maturation in the epididymis, as is the case for GOPC- and ZPBP1-null sperm (23, 25) because the type 4 sperm was barely found in the $Acrbp^{-/-}$ testis. When the morphology of $Acrbp^{-/-}$ sperm was further analyzed by TEM, the acrosome and nucleus showed structural abnormalities (Fig. 4*B*). All types of $Acrbp^{-/-}$ sperm possessed the deformed acrosome. Notably, the nucleus of type 2, type 3, and type 4 sperm was abnormally condensed, indicating that the defect in the nuclear condensation is accompanied by the loss of ACRBP. However, $Acrbp^{-/-}$ sperm as well as $Acrbp^{+/+}$ sperm contained the typical 9 + 2 microtubule axoneme in the flagella. Immunostaining analysis of $Acrbp^{-/-}$ sperm verified the aberrant localization of proACR, ZPBP2, ZPBP1, and SPACA1 on the head, although two acrosomal proteins, proACR and ZPBP2, were still present predominantly in the fragmented acrosomal vesicles (Fig. 4*C*). Thus, the loss of ACRBP-W and ACRBP-V5 in spermatids is linked to the abnormal structure of epididymal sperm.

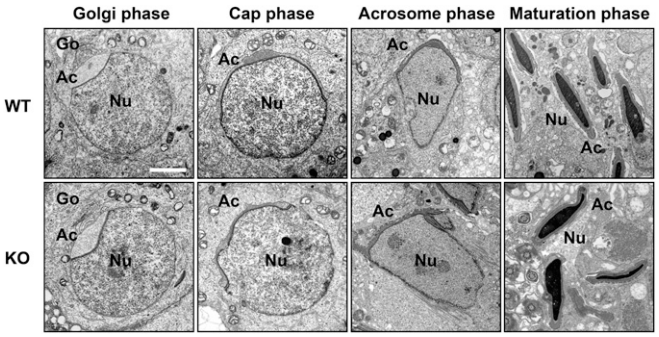

Fig. 3. Abnormal morphology of ACRBP-deficient spermatids. Ultrathin sections of spermatids from wild-type (WT) and ACRBP-deficient (KO) mice were analyzed by TEM. Ac, acrosomal vesicle; Go, Golgi apparatus; Nu, nucleus. (Scale bar, 2.0 μm.)

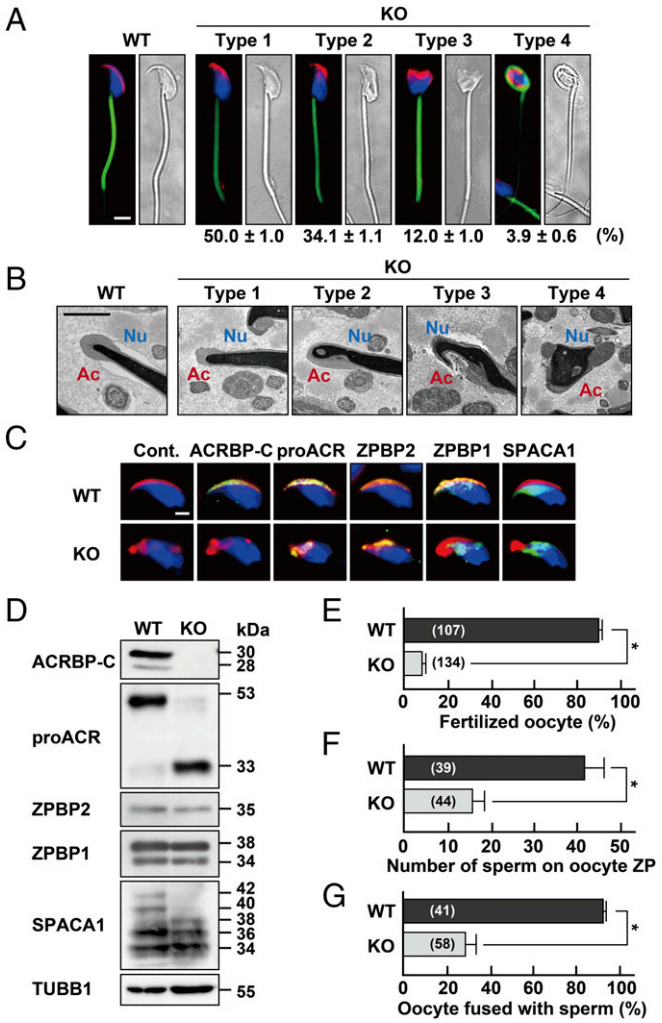

Fig. 4. Characterization of ACRBP-deficient epididymal sperm. (*A*) Sperm morphology. The acrosome, mitochondria, and nucleus of cauda epididymal sperm from wild-type (WT) and ACRBP-deficient (KO) mice were stained with fluorescent-dye–labeled PNA (red), MitoTracker Green FM (green), and Hochest 33342 (blue), respectively. The KO sperm were morphologically divided into four types, and the rate of each cell type was determined. (Scale bar, 4.0 μm.) (*B*) TEM analysis. Ac, acrosome; Nu, nucleus. (Scale bar, 1.0 μm.) (*C*) Immunostaining analysis. Sperm were immunostained with antibodies against proteins indicated (green) and also stained with fluorescent-dye–labeled PNA (red) and Hoechst 33342 (blue). No immunoreactive signal was detected when preimmune serum was used as the probe (Cont.). (Scale bar, 2.0 μm.) (*D*) Immunoblot analysis. Proteins were separated by SDS/PAGE and probed with antibodies against the sperm proteins indicated. (*E*–*G*) Functional assays of sperm. Capacitated sperm were subjected to assays for IVF (*E*), sperm/ZP binding (*F*), and sperm/oocyte fusion (*G*). The numbers in parentheses indicate those of the oocytes examined. All statistical significances are calculated using the Student *t* test. $^{*}P < 0.01$.

To examine whether acrosomal proteins, including proACR, are quantitatively and qualitatively affected by the loss of ACRBP, we carried out immunoblot analysis of protein extracts from epididymal sperm (Fig. 4*D*). Intriguingly, proACR was mostly processed into a mature form of ACR in $Acrbp^{-/-}$ sperm, whereas the levels of ZPBP1 and ZPBP2 were similar between $Acrbp^{+/+}$ and $Acrbp^{-/-}$ sperm. The 42- and 40-kDa forms of SPACA1 also exhibited a very low abundance in $Acrbp^{-/-}$ sperm. In addition, $Acrbp^{-/-}$ sperm normally contained five membrane proteins, IZUMO1 (10), zona pellucida (ZP)-binding protein ADAM3 (26), hyaluronidases SPAM1 and HYAL5 (27, 28), and GPI-anchored serine protease PRSS21 (29), as shown in Fig. S6. Thus, ACRBP is required for the maintenance of the enzymatically inactive ACR zymogen (pro-ACR) in the acrosome. It is also suggested that SPACA1 may be one of the target proteins for ACR.

We next examined the function of $Acrbp^{-/-}$ epididymal sperm. In vitro fertilization (IVF) assays using cumulus-intact oocytes indicated a pronounced defect of $Acrbp^{-/-}$ sperm in fertilizing the oocytes (Fig. 4*E*). The IVF rate in $Acrbp^{-/-}$ sperm was less than 10% of that in $Acrbp^{+/+}$ sperm. The abilities of $Acrbp^{-/-}$ sperm to bind the cumulus-free oocyte ZP and to fuse with the ZP-free oocytes were also diminished markedly (Fig. 4 *F* and *G*). Computer-assisted semen analysis (CASA) of capacitated epididymal sperm revealed that the rates of three parameters—total motility, rapid motility, and hyperactivation—in $Acrbp^{-/-}$ mice were significantly lower than those in $Acrbp^{+/+}$ mice (Table S1). Notably, $Acrbp^{-/-}$ sperm exhibited a remarkably high rate of static cells. We also examined the motility of each type of $Acrbp^{-/-}$ epididymal sperm by live imaging (Movie S1). Type 1 $Acrbp^{-/-}$ sperm were indistinguishable from the type 2 sperm based on morphology, without staining of the acrosome and nucleus. Compared with $Acrbp^{+/+}$ sperm, type 1/type 2 $Acrbp^{-/-}$ sperm were characterized by irregular patterns of flagellar beating and head rotations. The flagellar beating of the type 3 sperm was fairly dysfunctional, whereas the type 4 sperm displayed the loss in the forward movement. In addition to the aberrant flagellar beating, $Acrbp^{-/-}$ sperm, as well as mouse sperm lacking either one of catalytic subunit PPP3CC and regulatory subunit PPP3R2 of Ca^{2+}- and calmodulin-dependent serine-threonine phosphatase calcineurin (30), exhibited the defect in the bending motion of the midpiece. The frequencies of the midpiece bending in type 1/type 2 and type 3 $Acrbp^{-/-}$ sperm were modestly and severely reduced, respectively. The abnormal bending motion in $Acrbp^{-/-}$ sperm may be due to the deformed structure of the acrosome because ACRBP is localized exclusively in the acrosome (18). We could not examine the type 4 sperm, because of the entwinement of the midpiece around the nucleus (Fig. 4*A*). These data demonstrate the severely impaired function of $Acrbp^{-/-}$ sperm in vitro, consistent with the reduced fertility of $Acrbp^{-/-}$ male mice (Fig. 1*D*).

Globozoospermia, a severe form of teratozoospermia, is a human infertility syndrome characterized by a round-headed morphology of sperm without an acrosome (31, 32). The intracytoplasmic sperm injection (ICSI) treatment for globozoospermia patients results in a low success rate of fertilization, because of a reduced ability to activate the oocytes. In this study, we ascertained whether the oocytes are activated by ICSI using $Acrbp^{-/-}$ epididymal sperm (Fig. S7*A*). Most of the oocytes microinjected with the heads of type 1/type 2 or type 3 $Acrbp^{-/-}$ sperm (the whole cell for the type 4 sperm due to the failure to separate the head and tail) were successfully activated and reached the two-cell stage. All fetuses derived from $Acrbp^{-/-}$ sperm were verified to possess the *Acrbp*-null allele (Fig. S7*B*). Thus, despite the abnormal nuclear condensation, the nucleus of $Acrbp^{-/-}$ sperm is functionally active in pronuclear formation and subsequent embryonic development.

Production of Transgenic Mice Expressing Exogenous ACRBP-W or ACRBP-V5. We generated two transgenic mouse lines ($WT^{W\text{-}TG}$ and $WT^{V5\text{-}TG}$) expressing exogenous ACRBP-W and ACRBP-V5 under the control of the *Acrbp* promoter, respectively (Fig. 5*A*). The entire protein-coding region of ACRBP-W was designed to fuse with enhanced green fluorescent protein (EGFP). The transgenically expressed ACRBP-W-EGFP and ACRBP-V5 proteins also contained a myc-His tag at the C terminus. We randomly selected two lines each of $WT^{W\text{-}TG}$ (#3 and #51) and $WT^{V5\text{-}TG}$ (#22 and #31) mice from seven and five transgene-expressing lines, respectively (Fig. 5*B*).

Immunoblot analysis indicated that testicular extracts of $WT^{W\text{-}TG}$#3 and $WT^{W\text{-}TG}$#51 mice contain an 88/83-kDa doublet and a 58-kDa protein corresponding to myc-His–tagged

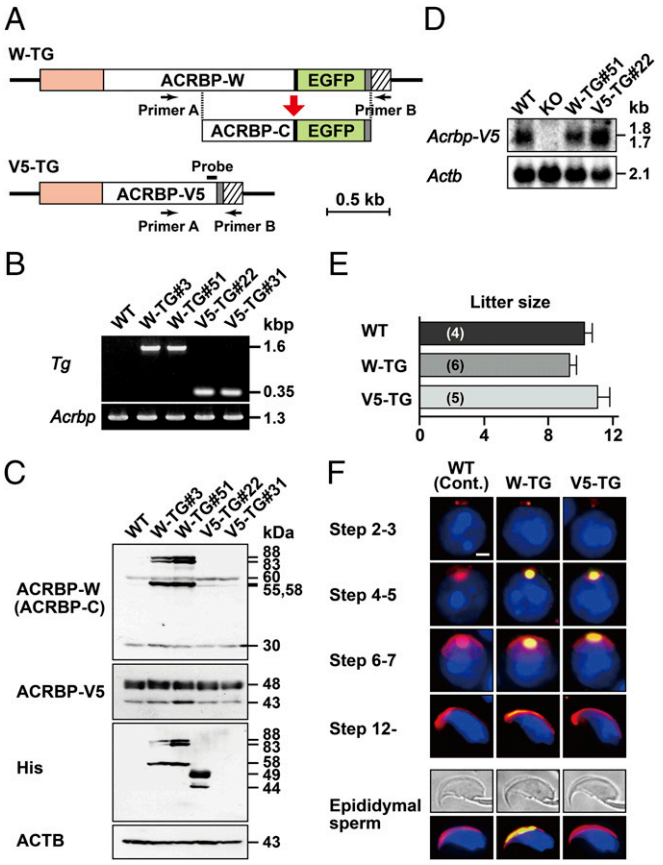

Fig. 5. Establishment and characterization of transgenic mouse lines expressing exogenous ACRBP-W or ACRBP-V5. (*A*) Transgene constructs. Two transgene constructs encoding ACRBP-W and ACRBP-V5 (W-TG and V5-TG, respectively) were designed to include the *Acrbp* promoter region (orange) at the 5′-end. The protein-coding regions of ACRBP-W, ACRBP-V5, and EGFP are indicated by open and green boxes, respectively. Closed, shaded, and hatched boxes represent the Gly-Gly-Ser-Gly-Gly linker, the myc-His tag, and the 3′-untranslated region of the bovine growth hormone gene, respectively. The location of a PCR primer set (primer A and primer B) is also indicated by arrows. (*B*) Agarose gel electrophoresis of PCR product. Two transgenic mouse lines, $WT^{W\text{-}TG}$ and $WT^{V5\text{-}TG}$, were established. PCR was carried out using tail genomic DNAs of each of the wild-type (WT), $WT^{W\text{-}TG}$#3, $WT^{W\text{-}TG}$#51, $WT^{V5\text{-}TG}$#22, and $WT^{V5\text{-}TG}$#31 mice as a template (*Tg*). Endogenous *Acrbp* as a control was also examined by PCR analysis (*Acrbp*). (*C*) Immunoblot analysis of testicular extracts. Proteins were probed with anti–ACRBP-C, anti–ACRBP-V5, anti–His-Tag, and anti-ACTB antibodies. (*D*) Northern blot analysis. Total cellular RNAs of testicular tissues from WT, ACRBP-deficient (KO), $WT^{W\text{-}TG}$#51, and $WT^{V5\text{-}TG}$#22 mice were probed with ^{32}P-labeled DNA fragment coding for ACRBP-V5 (*A*) or ACTB as probes. (*E*) Fertility of transgenic male mice. The WT, $WT^{W\text{-}TG}$#51, and $WT^{V5\text{-}TG}$#22 males (two different mice for each) were mated with WT females, and the litter sizes were counted. The males were all fertile. The numbers in parentheses indicate those of the WT females mated. (*F*) Immunostaining analysis. The subcellular localization of exogenously expressed ACRBP-W and ACRBP-V5 in spermatids and epididymal sperm was examined by immunostaining with anti-Myc antibody (green). No immunoreactive signal was detected in WT spermatids and sperm when preimmune serum was used as the probe (Cont.). Cells were also counterstained with fluorescent-dye–labeled PNA (red) and Hoechst 33342 (blue). (Scale bar, 2.0 μm.)

ACRBP-W-EGFP and ACRBP-C-EGFP, respectively (Fig. 5*C*), in addition to endogenous 60/55-kDa ACRBP-W and 30-kDa ACRBP-C (18). The levels of ACRBP-W-EGFP and ACRBP-C-EGFP in the $WT^{W\text{-}TG}$#3 and $WT^{W\text{-}TG}$#51 testes were more than threefold higher than those of endogenous ACRBP-W and ACRBP-C in the wild-type, $WT^{W\text{-}TG}$#3, and $WT^{W\text{-}TG}$#51 testes. When the blots were probed with anti–ACRBP-V5 antibody, the abundance of endogenous ACRBP-V5 as a 48/43-kDa doublet (18) was comparable among wild-type and four transgenic mice including $WT^{V5\text{-}TG}$#22 and $WT^{V5\text{-}TG}$#31 mice. Because no immunoreactive band corresponding to exogenously expressed ACRBP-V5 tagged with myc-His was detectable, we used anti-His antibody as a probe (Fig. 5*C*). A doublet of 49- and 44-kDa myc-His–tagged ACRBP-V5 proteins was found only in the $WT^{V5\text{-}TG}$#22 testis, indicating that anti–ACRBP-V5 antibody raised against the C-terminal seven-residue peptide of ACRBP-V5 (18) poorly recognizes myc-His–tagged ACRBP-V5. To estimate the expression level of exogenous ACRBP-V5, we carried out Northern blot analysis of testicular total RNAs (Fig. 5*D*). The level of *Acrbp-V5* mRNA in $WT^{V5\text{-}TG}$#22 testis was approximately twice as abundant as those in the wild-type and $WT^{W\text{-}TG}$#51 testes. Assuming that the $WT^{V5\text{-}TG}$#22 testis contains a mixture of endogenously and exogenously expressed *Acrbp-V5* mRNAs with approximate sizes of 1.7 and 1.8 kb, respectively, these two mRNAs are equivalently expressed in the $WT^{V5\text{-}TG}$#22 testis. We thus selected $WT^{W\text{-}TG}$#51 and $WT^{V5\text{-}TG}$#22 transgenic mice for further analysis.

$WT^{W\text{-}TG}$#51 and $WT^{V5\text{-}TG}$#22 males were all fertile and produced normal litter sizes when mated with wild-type females (Fig. 5*E*). Immunostaining analysis verified that acrosome formation in spermatids of the $WT^{W\text{-}TG}$#51 and $WT^{V5\text{-}TG}$#22 testes is normal (Fig. 5*F*). The localization of exogenously expressed ACRBP-W-EGFP and ACRBP-V5 in acrosomal vesicles was similar to those of endogenous ACRBPs (Figs. 2*C* and 5*F*). Consistent with our previous data (18), no exogenous ACRBP-V5 was found in the acrosome of cauda epididymal sperm. Thus, acrosome formation is unaffected by transgenic expression of ACRBP-W-EGFP and ACRBP-V5 in spermatids.

Rescue of Phenotypical Abnormality in ACRBP-Deficient Mice. To examine whether the phenotypical abnormality of $Acrbp^{-/-}$ mice is rescued by transgenic introduction of ACRBP-W-EGFP or ACRBP-V5 into the knockout background, $Acrbp^{-/-}$ mice carrying the *Acrbp-W-EGFP* (termed $KO^{W\text{-}TG}$) or *Acrbp-V5* transgene ($KO^{V5\text{-}TG}$) were obtained by crossing between $Acrbp^{-/-}$ and $WT^{W\text{-}TG}$#51 or $WT^{V5\text{-}TG}$#22 mice and then by mating the F1 males with $Acrbp^{-/-}$ females. Mating of $KO^{V5\text{-}TG}$ male mice with wild-type females resulted in an average litter size similar to that obtained by the wild-type pairs (Fig. 6*A*). $KO^{W\text{-}TG}$ males also exhibited a significant increase in the litter sizes compared with $Acrbp^{-/-}$ males. The impaired fertility of $Acrbp^{-/-}$ epididymal sperm in vitro was recovered moderately and greatly by exogenous expression of ACRBP-W-EGFP and ACRBP-V5, respectively (Fig. 6*B*). Formation of acrosomal granules was normal in $KO^{W\text{-}TG}$ and $KO^{V5\text{-}TG}$ spermatids at the Golgi phase (Fig. 6*C*). Importantly, the fragmented acrosomal structure of elongating spermatids and epididymal sperm in $Acrbp^{-/-}$ mice was recovered to a nearly normal level by exogenous ACRBP-V5 expression. Similarly to ZPBP1-null spermatids (23), the acrosomal granules in $KO^{W\text{-}TG}$ spermatids were eccentrically localized in the acrosomal vesicle at the cap phase. Indeed, immunostaining of $KO^{W\text{-}TG}$ spermatids revealed that spermatogenic cell-specific proteins, including pro-ACR and ZPBP2, in acrosomal granules are not distributed in the center of acrosomal vesicles (Fig. 6*D*). When the acrosome and nucleus of epididymal sperm from $KO^{V5\text{-}TG}$ mice were stained with fluorescent probes, ∼90% of total $KO^{V5\text{-}TG}$ sperm displayed a morphology comparable to that of wild-type sperm (Fig. S8). However, $KO^{W\text{-}TG}$ mice possessed only a limited number of wild-type–like sperm (almost 18% of total cells) and still contained type 1, type 2, type 3, and type 4 sperm at the rates of 22%, 31%, 16%, and 13%, respectively. Thus, ACRBP-V5 plays a crucial role in the formation and configuration of the acrosomal granule during spermiogenesis. It is also suggested that ACRBP-W partially contributes to acrosomal granule formation and is not

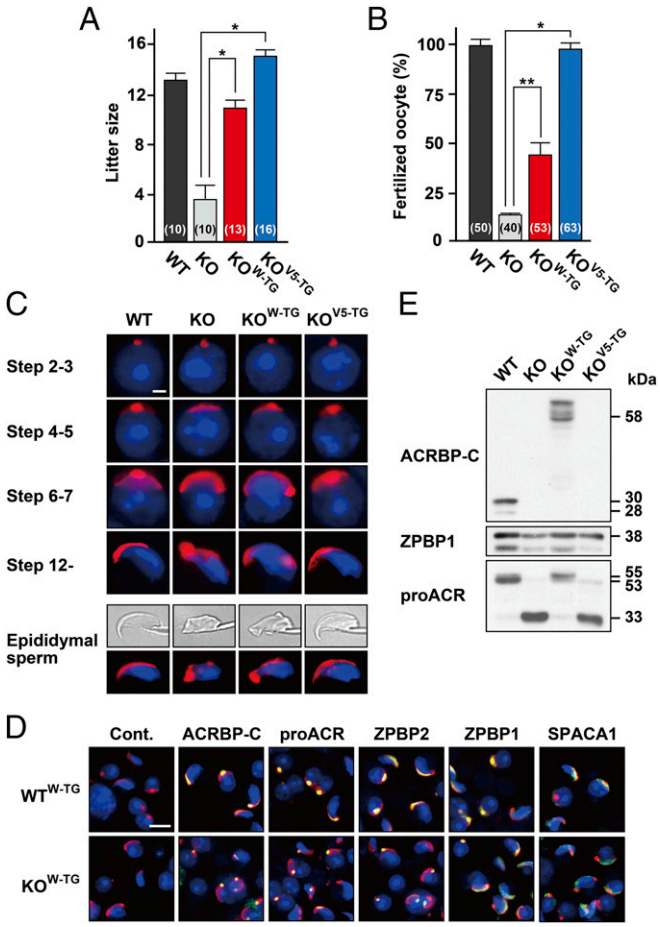

Fig. 6. Rescue of phenotypical abnormality in ACRBP-deficient spermatids by transgenic expression of ACRBP-W or ACRBP-V5. (*A*) Fertility. ACRBP-deficient (KO) male mice carrying the ACRBP-W and ACRBP-V5 transgenes ($KO^{W\text{-}TG}$ and $KO^{V5\text{-}TG}$ mice, respectively) were generated. The wild-type (WT), KO, $KO^{W\text{-}TG}$, and $KO^{V5\text{-}TG}$ males (three, three, three, and four different mice, respectively) were mated with WT females, and the litter sizes were counted. The male mice examined were all fertile. The numbers in parentheses indicate those of the WT females mated. All statistical significances are calculated using the Student *t* test. $*P < 0.01$. (*B*) IVF assays. Capacitated cauda epididymal sperm were subjected to IVF assays using the cumulus-intact oocytes. The numbers in parentheses indicate those of the oocytes examined. $**P < 0.05$; $*P < 0.01$. (*C*) Morphological analysis. Spermatids and cauda epididymal sperm were stained with fluorescent-dye–labeled PNA (red) and Hoechst 33342 (blue). (Scale bar, 2.0 μm.) (*D*) Subcellular localization of acrosomal proteins. Spermatids were immunostained with antibodies against the proteins indicated (green). The acrosome and nucleus were also stained with fluorescent-dye–labeled PNA (red) and Hoechst 33342 (blue), respectively. No immunoreactive signal was detected when preimmune serum was used as the probe (Cont.). (Scale bar, 8.0 μm.) (*E*) Immunoblot analysis. Proteins of epididymal sperm extracts from WT, KO, $KO^{W\text{-}TG}$, and $KO^{V5\text{-}TG}$ mice were probed with anti–ACRBP-C, anti-proACR, and anti-ZPBP1 antibodies.

implicated in the configuration of the acrosomal granule in the acrosomal vesicle.

We also asked whether aberrant processing of proACR in $Acrbp^{-/-}$ epididymal sperm (Fig. 4*D*) occurs when either ACRBP-W-EGFP or ACRBP-V5 is exogenously expressed. Immunoblot analysis of epididymal sperm extracts revealed that proACR remains unprocessed in $KO^{W\text{-}TG}$ mice (Fig. 6*E*). In contrast, proACR in $KO^{V5\text{-}TG}$ sperm was converted mostly to a 33-kDa form of ACR, similarly to $Acrbp^{-/-}$ sperm. These data suggest that ACRBP-C functions in the maintenance of proACR as an enzymatically inactive ACR zymogen in the acrosome.

Discussion

This study describes the functional specialization of two ACRBP proteins, ACRBP-W and ACRBP-V5, that are produced by pre-mRNA alternative splicing in the mouse (18). The $Acrbp^{-/-}$ male mice lacking both ACRBP-W and ACRBP-V5 show a severely reduced fertility (Fig. 1), because of aberrant formation of the acrosome (Figs. 2 and 3). Although proacrosomal vesicles normally assemble, $Acrbp^{-/-}$ early spermatids fail to form a large acrosomal granule (Fig. 2). The impaired ability to produce the acrosomal granule in the $Acrbp^{-/-}$ spermatids is linked to the fragmented structure of the acrosome, further leading to the abnormally round-headed shape structure and reduced motility of $Acrbp^{-/-}$ epididymal sperm (Fig. 4 and Table S1). The aberrant formation of the acrosomal granule is recovered by transgenic expression of either ACRBP-W or ACRBP-V5 in $Acrbp^{-/-}$ spermatids, although exogenous ACRBP-W expression results in the eccentric localization of the acrosomal granule in the acrosome vesicle (Fig. 6). Moreover, transgenic introduction of ACRBP-W maintains proACR as an enzymatically inactive zymogen in the acrosome by preventing the zymogen from processing into a mature form of ACR (Fig. 6). Thus, ACRBP-V5 plays the key role in the formation and configuration of the acrosomal granule into the center of the acrosomal vesicle during early spermiogenesis. ACRBP-W also seems to partially contribute to the acrosomal granule formation. However, because ACRBP-W is immediately processed into ACRBP-C in spermatids (18), the major role of ACRBP-W is the retention of the inactive status of proACR in the acrosome through the ACRBP-C function, in addition to the promotion of ACR release from the acrosome during acrosomal exocytosis (14, 18), as described in Fig. 7 and Fig. S1.

Deletions and mutations in some human genes, including *SPATA16*, *PICK1*, *DPY19L2*, and *ZPBP1*, have been identified in globozoospermia patients (33–38). Gene-knockout mice, including ZPBP1-null (23), SPACA1-null (24), and GOPC-null mice (25), are known to exhibit the phenotype similar to that of human globozoospermia (39–47). Our data indicate that a small population (~4%) of $Acrbp^{-/-}$ epididymal sperm are round-headed but still possess the fragmented acrosome on the head (Fig. 4), thus suggesting that ACRBP may not be directly involved in the globozoospermia-related phenotype. Of the mutant mice relating to globozoospermia, the acrosome is completely deficient in the $Gopc^{-/-}$ mice (25). As described above, $Zpbp1^{-/-}$ mice exhibit the eccentric localization of the acrosomal granule in spermatids (23), whereas early spermatids of $Spaca1^{-/-}$ mice apparently lack the acrosomal granule in the acrosome (24). The phenotypes of $Zpbp1^{-/-}$ and $Spaca1^{-/-}$ spermatids resemble those of $KO^{W\text{-}TG}$ and $Acrbp^{-/-}$ spermatids, respectively. However, the abnormally developing acrosome is gradually lost from the $Zpbp1^{-/-}$ and $Spaca1^{-/-}$ spermatids at later stages of spermiogenesis (23, 24). The levels of ZPBP1 and SPACA1 are significantly low in the $Gopc^{-/-}$ testis (24). Despite a normal level of ZPBP1 in the $Spaca1^{-/-}$ testis, the $Zpbp1^{-/-}$ testis exhibits a greatly reduced level of SPACA1 (24). Importantly, the $Acrbp^{-/-}$ testis normally contains globozoospermia-related proteins, including GOPC, ZPBP1, and SPACA1 (Fig. S3). Thus, the reason why $Acrbp^{-/-}$ spermatids and epididymal sperm still contain the fragmented acrosome may be due to the fact that ACRBP is localized exclusively in the acrosomal matrix, together with proACR (5). Because ZPBP1 and SPACA1 are an inner acrosomal membrane-associated protein and an integral acrosomal membrane protein, respectively (23, 24), it appears that the functional role of ACRBP may be spatiotemporally different from those of GOPC, ZPBP1, and SPACA1 during acrosome formation. We note that the loss of functional ACRBP in human globozoospermia and teratozoospermia patients still remains an open question. Thus, it is important to evaluate the gene mutations in the future.

The phenotype of $KO^{W\text{-}TG}$ mice is also similar to that of proprotein covertase subtilisin/kexin type 4 (PCSK4; also known

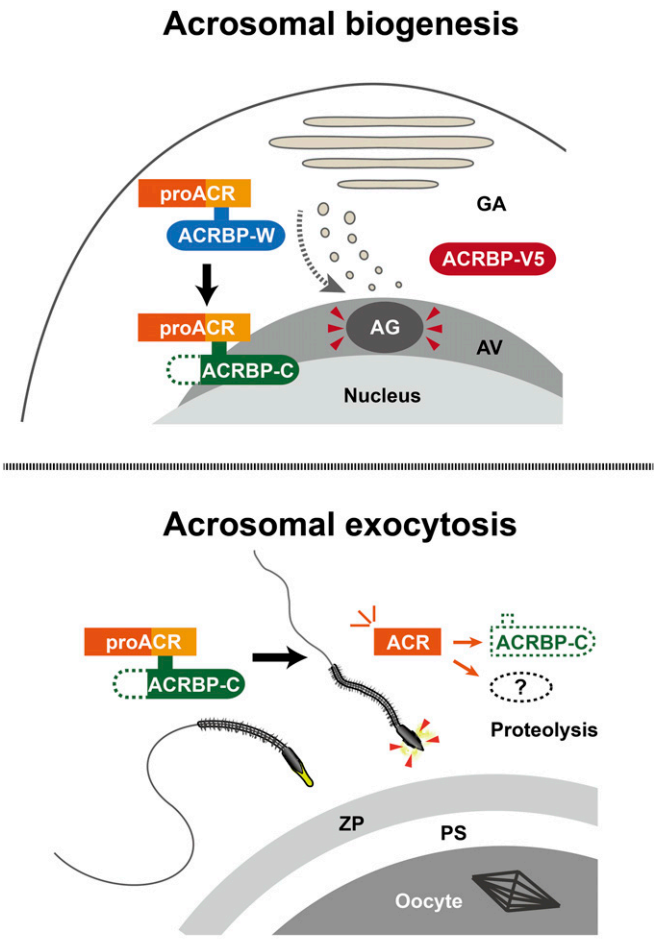

Fig. 7. Functional roles of mouse ACRBP in spermiogenesis and fertilization. ACRBP-V5 functions in the formation and configuration of an acrosomal granule in round spermatids (*Upper*). Because ACRBP-V5 is proteolytically degraded in elongating spermatids (18), this protein may be also involved in the enlargement/elongation of the acrosomal granule. ACRBP-W is synthesized in haploid spermatids and then immediately converted into ACRBP-C by removal of the N-terminal half (18). The major function of ACRBP-W and ACRBP-C is to retain the inactive status of proACR in the acrosomal granule, although ACRBP-W partially contributes to the assembly of acrosomal proteins, including proACR, to form an acrosomal granule. In the fertilization process (*Lower*), sperm contain only ACRBP-C that promotes ACR release from the acrosome during acrosomal exocytosis. Acrosomal components, including ACRBP-C, are probably degraded by enzymatically active ACR that is released. AG, acrosomal granule; AV, acrosomal vesicle; GA, Golgi apparatus; PS; perivitelline space; ZP, zona pellucida.

as PC4 or SPC5)-null mice (48): the abnormally eccentric localization of the acrosomal granule and the fragmented structure of acrosome. The loss of PCSK4 results in the failure of ACRBP-W proteolytic processing into the mature ACRBP-C in testicular and epididymal sperm (48), implying that the failure of ACRBP-W processing in *Pcsk4*$^{-/-}$ spermatids may be attributed to abnormal formation of the acrosome. However, despite the phenotypical similarity between the *Pcsk4*$^{-/-}$ and KO$^{W\text{-}TG}$ mice, exogenously expressed ACRBP-W in spermatids and sperm is normally converted into ACRBP-C (Figs. 5 and 6). These results suggest that the ACRBP-W processing, which is presumably catalyzed by PCSK4 directly or indirectly (48), may not be involved in the observed phenotypes of *Pcsk4*$^{-/-}$ and KO$^{W\text{-}TG}$ mice. On the other hand, the concentric localization of acrosomal granule is recovered only by transgenic expression of ACRBP-V5 in *Acrbp*$^{-/-}$ spermatids (Fig. 6). As described previously (18), ACRBP-V5 is present in the acrosomal granules of round spermatids and then is proteolytically degraded in elongating spermatids. Thus, our present data suggest a possible involvement of ACRBP-V5 in the enlargement/elongation of the acrosomal granule in the acrosome of elongating spermatids; the retention of acrosomal proteins in the acrosomal granule may be released by the disappearance of ACRBP-V5. Indeed, the time period for the appearance and disappearance of ACRBP-V5 matches well with that for the dynamic changes in the structure of acrosomal granule (Fig. 2). Moreover, because the protein sequence of ACRBP-V5 is distinguished from that of ACRBP-W by only five amino acids at the C terminus (Fig. S9), the 5-residue sequence probably acts as the key determinant of the ACRBP-V5 function. How ACRBP-V5 is degraded by proteolytic enzymes, including PCSK4, in spermatids remains to be answered.

We (14, 18) previously demonstrated that, although two transcripts encoding ACRBP-W and ACRBP-V5 are generated in the mouse testis, the pig and guinea pig testes produce only a single mRNA coding for ACRBP-W. A single *ACRBP-W* mRNA is also transcribed in the human testis (15). Our preliminary experiments indicated that *Acrbp-V5* mRNA, in addition to *Acrbp-W* mRNA, is produced specifically in rodent animals, including rat and hamster. One of the most puzzling questions is whether the single ACRBP-W protein in human, pig, and guinea pig serves the functions of both ACRBP-W and ACRBP-V5 in the mouse. The amino acid sequence of mouse ACRBP-W shares 71–75% identity with those of the human, pig, and guinea pig proteins, whereas the sequence identity of ACRBP-W is around 80% among the three nonrodent animals (Fig. S9). It is thus conceivable that the functional diversity of ACRBP-W is not merely explained by the sequence alignment. Meanwhile, rodent animal sperm usually possess a falciform-shaped head, whereas the heads of pig, guinea pig, and human sperm are spatulate (1, 2). The morphological variation of the sperm heads between rodent and nonrodent animals presumably reflects the difference in the enlargement/elongation of the acrosomal granule in the acrosomal vesicle. If so, ACRBP-V5 may not be essential for the acrosome formation in nonrodent animals. Another possibility is that the time for ACRBP-W conversion into ACRBP-C differs between rodent and nonrodent animals. Although ACRBP-W is immediately processed into ACRBP-C in early spermatids in the mouse (18), the proteolytic processing may occur at later stages of spermiogenesis or during epididymal sperm maturation in the nonrodent animals. In this case, the lack of ACRBP-V5 in nonrodent animals can be compensated by the unprocessed form of ACRBP-W. To explore these possibilities, further studies are required. At any rate, our present study provides an example of cell organellar biogenesis regulated by pre-mRNA alternative splicing.

Materials and Methods

Generation of Mutant Mice Lacking ACRBP. A targeting vector containing an expression cassette (49) of *neo* flanked by ~1.3- and 6.5-kbp genomic regions of *Acrbp* at the 5′- and 3′-ends, respectively, was constructed as described previously (50). The MC1 promoter-driven herpes simplex virus thymidine kinase gene (*tk*) was also inserted into the 6.5-kbp *Acrbp* genomic region at the 3′-end. Following electroporation of the targeting vector, which had been linearized by digestion with NotI, into mouse D3 ES cells, homologous recombinants were selected using G418 and gancyclovir as described previously (50). Five ES cell clones carrying the targeted mutation were selected and injected into blastocysts of C57BL/6 mice (Japan SLC). The blastocysts were transferred to pseudopregnant foster mothers to obtain chimeric male mice. The male mice were crossed to ICR (Institute of Cancer Research)-strain females (Japan SLC) to establish mouse lines heterozygous for the *Acrbp* mutation. The homozygous mice were obtained by mating of the heterozygous males and females. All animal experiments were performed ethically, and experimentation was in accord with the Guide for the Care and Use of Laboratory Animals at University of Tsukuba.

Establishment of Transgenic Mouse Lines Expressing Exogenous ACRBP-W or ACRBP-V5. The 500-bp 5′-flanking region of *Acrbp* was amplified by PCR, and the DNA fragment was ligated to the cDNA fragment encoding ACRBP-W or ACRBP-V5. The ACRBP-W construct was also designed to fuse with a linker, Gly-Gly-Ser-Gly-Gly (51), and EGFP at the C terminus. These two transgene constructs were introduced into appropriate restriction endonuclease sites of pcDNA3.1-myc-His (Thermo Fisher Scientific) and digested with restriction enzymes. The linearized DNA fragments were then microinjected into pronuclei of one-cell embryos from BDF1 mice (Japan SLC) to establish transgenic mouse lines, as described previously (52). Transmission of the transgenes in founder mouse lines was validated by PCR of tail DNAs using a set of two oligonucleotide primers (primer A: 5′-TCAGAGCCCAAGTTTCAATC-3′; primer B: 5′-TAGAAGGCACAGTCGAGG-3′). The founder mice were bred with ICR mice to establish stable transgenic lines that were maintained by mating with ICR mice.

Hybridization Analysis. Genomic DNA was prepared from mouse tail, digested by BamHI, separated by agarose gel electrophoresis, and transferred onto Hybond-N^+ nylon membranes (GE Healthcare Bio-Sciences). Total cellular RNAs were extracted from testicular tissues using Isogen (Nippon Gene) as described previously (53). The RNA samples were glyoxylated, separated by electrophoresis on agarose gels, and transferred onto nylon membranes. Hybridization was carried out as described previously (53).

Preparation of Protein Extracts. Testicular tissues of mice (3–5 mo old) were homogenized at 4 °C in a lysis buffer, pH 7.4, consisting of 20 mM Tris·HCl, 0.15 M NaCl, 1% Triton X-100, 0.5 mM DTT, 0.5 mM phenylmethanesulfonyl fluoride, 1 μg/mL pepstatin A, 1 μg/mL leupeptin, and 75 U/mL aprotinin, using a Potter-Elvehjem glass homogenizer (AS ONE Co.) fitted with a Teflon pestle (10 strokes). Cauda epididymal sperm were lysed in the same lysis buffer by pipetting at 4 °C. The homogenates were centrifuged at 11,200 × *g* for 10 min at 4 °C. The supernatant solution was used as a source of protein extracts. Protein concentration was determined using a Coomassie protein assay reagent kit (Thermo Fisher Scientific).

Antibodies. His-tagged recombinant ZPBP1 and ZPBP2 containing the amino acid sequences at positions 101–406 and 22–253, respectively, were produced in *Escherichia coli* BL21 (DE3), as described previously (18, 23). The recombinant proteins were purified on a Ni-NTA His column (Merck Millipore), emulsified with Freund's complete (Becton Dickenson) or incomplete adjuvant (Wako), and injected into female New Zealand White rabbits (SLC). Antibodies were affinity-purified on Sepharose 4B columns previously coupled with GST-tagged recombinant ZPBP1 and ZPBP2 as described previously (18). Polyclonal antibodies against ACRBP-C, ACRBP-V5, ACR, SPAM1, HYAL5, ADAM3, IZUMO1, and SPACA1 were prepared as described previously (10, 18, 24, 27, 28, 54, 55). Anti-ACTB (clone AC-15) and anti-TUBB1 (clone 2-28-33) monoclonal antibodies were purchased from Sigma-Aldrich. Anti-His-Tag, anti-GOPC/PIST, anti-HRB/AGFG1, anti-PRSS21/TESP5, and anti-Myc (clone 9E10) antibodies were the products of Medical and Biological Laboratories, Abcam, Proteintech, Santa Cruz Biotechnology, and ThermoFisher Scientific, respectively. Horseradish peroxidase-conjugated antibodies against rabbit, mouse, or goat IgG (H + L) were purchased from Jackson Immunoresearch Laboratories. Alexa Fluor 488-conjugated antibodies against rabbit or mouse IgG were purchased from Thermo Fisher Scientific.

Immunoblot Analysis. Proteins were separated by SDS/PAGE and transferred onto Immobilon-P polyvinylidene difluoride membranes (Merck Millipore). The blots were blocked with 4% (wt/vol) skim milk in 20 mM Tris·HCl, pH 7.5, containing 0.1% Tween-20 and 0.15 M NaCl at room temperature for 1 h, incubated with primary antibodies at room temperature for 1 h, and then treated with secondary antibodies conjugated with horseradish peroxidase at room temperature for 1 h. The immunoreactive proteins were visualized by using an ECL Western Blotting Detection kit (GE Healthcare Bio-Sciences), followed by exposure to X-ray films (Fujifilm).

Immunostaining Analysis. Cauda epididymal sperm were dispersed in a 0.2-mL drop of TYH (Toyoda–Yokoyama–Hoshi) medium (56) free of BSA. The sperm suspension was transferred into a 1.5-mL microtube, washed with PBS by centrifugation at 800 × *g* for 5 min, fixed in 4% (wt/vol) paraformaldehyde in PBS, pH 7.2, on ice for 15 min, washed with cold PBS, and then treated with 0.1% Triton X-100 in PBS at room temperature for 15 min. The fixed cells were blocked with 3% (vol/vol) normal goat serum in PBS containing 0.05% Tween-20 on ice for 30 min, washed with the same buffer, incubated with primary antibodies for 1 h, washed, and then reacted with Alexa Fluor 488-conjugated anti-rabbit or mouse IgG antibody for 1 h. After washing with PBS, sperm cells were incubated with Alexa Fluor 568-conjugated PNA (3 μg/mL; Thermo Fisher Scientific) and Hoechst 33342 (2.5 μg/mL; Thermo Fisher Scientific) for 30 min, washed with PBS, mounted, and then observed under an IX-71 fluorescence microscope (Olympus), as described previously (57). Spermatogenic cells were prepared from seminiferous tubules as described previously (58). After blocking with 3% (vol/vol) normal goat serum in PBS containing 0.05% Tween-20, the cell samples were treated with primary antibodies, reacted with Alexa Fluor 488-conjugated anti-rabbit or mouse IgG antibody, incubated with Alexa Fluor 568-labeled PNA and Hoechst 33342, and then observed, as described above.

TEM Analysis. Fresh tissues of cauda epididymides and testes were fixed in 2.5% (vol/vol) glutaraldehyde in 0.1 M phosphate buffer (PB), pH 7.4, for 30 min at room temperature, washed with PB, postfixed in 1% osmium tetroxide for 30 min at 4 °C, dehydrated in ethanol, and embedded in Epon. Ultrathin sections (90 nm) were prepared by using a Reichert-Jung Ultracut E ultramicrotome (Reichert Technologies, Inc.), stained with uranyl acetate and lead citrate, and then observed under a JEM1400 TEM (JEOL) at 80-kV accelerating voltage.

CASA. Parameters of sperm motility were quantified by CASA using an integrated visual optical system (IVOS) software (Hamilton-Thorne Biosciences) as described previously (59). Briefly, cauda epididymal sperm were capacitated by incubation for 2 h in a 0.1-mL drop of TYH medium at 37 °C under 5% (vol/vol) CO_2 in air. An aliquot of the capacitated sperm suspension was transferred into a prewarmed counting chamber (depth = 20 μm), and more than 200 sperm were examined for each sample using standard settings (30 frames acquired at a frame rate of 60 Hz at 37 °C) as described previously (60, 61). Hyperactivated motility of sperm was determined by using the SORT function of the IVOS software (61). Sperm were classified as "hyperactivated" when the trajectory met the following criteria (61): curvilinear velocity ≥ 180 μm/s, linearity ≤ 38%, and amplitude of lateral head displacement ≥ 9.5 μm.

IVF Assays. ICR mice (8–10 wk old) were superovulated by intraperitoneal injection of pregnant mare's serum gonadotropin (5 units; Aska Pharmaceutical Co.) followed by human CG (hCG) (5 units; Aska Pharmaceutical) 48 h later. The cumulus-intact metaphase II-arrested oocytes were isolated from the oviductal ampulla of superovulated mice 14 h after hCG injection and placed in a 90-μL drop of TYH medium. Cauda epididymal sperm were capacitated by incubation in a 0.1-mL drop of TYH medium for 2 h at 37 °C under 5% (vol/vol) CO_2 in air. An aliquot (1.5×10^4 cells/10 μL) of the capacitated sperm suspension was mixed with the above-mentioned 90-μL drop of TYH medium containing the oocytes to give a final concentration of 1.5×10^2 sperm/μL. The mixture (0.1 mL) was incubated for 6 h at 37 °C under 5% (vol/vol) CO_2 in air. The fertilized oocytes were treated with bovine testicular hyaluronidase (350 units/mL; Sigma-Aldrich) for 10 min to remove cumulus cells, fixed in PBS containing 4% (wt/vol) paraformaldehyde and 0.5% polyvinylpyrrolidone (PVP), and washed with PBS containing 0.5% PVP. The female and male pronuclei in the fertilized oocytes were stained with Hoechst 33342 (2.5 μg/mL) and then viewed under an IX-71 fluorescence microscope as described previously (59).

Sperm/ZP-Binding Assays. The cumulus-free, ZP-intact oocytes were prepared by treatment with bovine testicular hyaluronidase for 15 min, washed with TYH medium, and placed in a 90-μL drop of TYH medium. Capacitated epididymal sperm (3.0×10^4 cells/10 μL) were mixed with the 90-μL drop containing the cumulus-free oocytes and two-cell embryos, and the mixture (0.1 mL) was incubated for 30 min at 37 °C under 5% (vol/vol) CO_2 in air. The oocytes were transferred to a 0.1-mL drop of TYH medium, washed by pipetting to remove loosely bound and unbound sperm, fixed in PBS containing 4% (wt/vol) paraformaldehyde and 0.5% PVP for 15 min, and washed with PBS containing 0.5% PVP. After staining with Hoechst 33342 (2.5 μg/mL), the numbers of sperm tightly bound to the ZP were counted under an Olympus IX-71 fluorescence microscope, as described previously (59). The two-cell embryos were used as an internal negative control for nonspecific and loose sperm binding.

Sperm/Oocyte Fusion Assays. The cumulus-free, ZP-intact oocytes were treated with acid Tyrode (Sigma-Aldrich), washed with TYH medium, treated with Hoechst 33342 (2.5 μg/mL) for 10 min, and washed three times with TYH medium as described previously (59). The Hoechst-labeled, ZP-free oocytes in a 90-μL drop of TYH medium were mixed with capacitated epididymal sperm (1.5×10^4 cells/10 μL), and the mixture (0.1 mL) was incubated for 30 min at 37 °C under 5% (vol/vol) CO_2 in air. The oocytes were washed with PBS containing 0.5% PVP, fixed in PBS containing 0.25% glutaraldehyde and 0.5% PVP, and then observed under an Olympus IX-71 fluorescence microscope.

ICSI. ICSI was carried out according to the already published procedure (62), using a micropipette attached to a Piezo-electric actuator (PrimeTech). Briefly, a single epididymal sperm was sucked into an injection pipette, and the sperm head was separated from the tail by applying a few Piezo pulses to the head–tail junction. The cumulus-free oocytes were prepared from superovulated BDF1 mice (Japan SLC) as described above. The sperm head was injected into the oocyte in Hepes-buffered CZB (Chatot–Ziomek–Bavister) medium (63). Type 4 *Acrbp*$^{-/-}$ sperm, the head and tail of which could not be separated by Piezo pulses, were injected into the oocyte as the whole cell. The injected oocytes were cultured in CZB medium at 37 °C for 24 h under 5% (vol/vol) CO_2 in air. Embryos that reached the two-cell stage were transferred into the oviducts of pseudopregnant ICR mice on the day after sterile mating with a vasectomized male (day 0.5). On day 19.5, the uteri of the recipient mice were examined for the presence of live term fetuses.

Statistical Analysis. Data are represented as the mean ± SE ($n \geq 3$). The Student *t* test was used for statistical analysis; significance was assumed for $P < 0.05$.

ACKNOWLEDGMENTS. We thank the NPO Biotechnology Research and Development for generation of mutant mice, and Ms. J. Sakamoto for transmission electron microscope analysis. This work was supported in part by grants from the Japan Society for the Promotion of Science and the Ministry of Education, Culture, Sports, Science and Technology in Japan (to Y. Kanemori and T.B.).

1. Leblond CP, Clermont Y (1952) Spermiogenesis of rat, mouse, hamster and guinea pig as revealed by the periodic acid-fuchsin sulfurous acid technique. *Am J Anat* 90(2): 167–215.
2. Yanagimachi R (1994) Mammalian fertilization. *The Physiology of Reproduction*, eds Kobil E, Neill JD (Raven Press, New York), Vol 1, pp 189–317.
3. Abou-Haila A, Tulsiani DR (2000) Mammalian sperm acrosome: Formation, contents, and function. *Arch Biochem Biophys* 379(2):173–182.
4. Kierszenbaum AL, Tres LL (2004) The acrosome-acroplaxome-manchette complex and the shaping of the spermatid head. *Arch Histol Cytol* 67(4):271–284.
5. Buffone MG, Foster JA, Gerton GL (2008) The role of the acrosomal matrix in fertilization. *Int J Dev Biol* 52(5-6):511–522.
6. Okabe M (2013) The cell biology of mammalian fertilization. *Development* 140(22): 4471–4479.
7. Kim KS, Gerton GL (2003) Differential release of soluble and matrix components: Evidence for intermediate states of secretion during spontaneous acrosomal exocytosis in mouse sperm. *Dev Biol* 264(1):141–152.
8. Baba T, Azuma S, Kashiwabara S, Toyoda Y (1994) Sperm from mice carrying a targeted mutation of the acrosin gene can penetrate the oocyte zona pellucida and effect fertilization. *J Biol Chem* 269(50):31845–31849.
9. Yamagata K, et al. (1998) Acrosin accelerates the dispersal of sperm acrosomal proteins during acrosome reaction. *J Biol Chem* 273(17):10470–10474.
10. Inoue N, Ikawa M, Isotani A, Okabe M (2005) The immunoglobulin superfamily protein Izumo is required for sperm to fuse with eggs. *Nature* 434(7030):234–238.
11. Bianchi E, Doe B, Goulding D, Wright GJ (2014) Juno is the egg Izumo receptor and is essential for mammalian fertilization. *Nature* 508(7497):483–487.
12. Baba T, Michikawa Y, Kashiwabara S, Arai Y (1989) Proacrosin activation in the presence of a 32-kDa protein from boar spermatozoa. *Biochem Biophys Res Commun* 160(3):1026–1032.
13. Hardy DM, Oda MN, Friend DS, Huang TT, Jr (1991) A mechanism for differential release of acrosomal enzymes during the acrosome reaction. *Biochem J* 275(Pt 3): 759–766.
14. Baba T, et al. (1994) An acrosomal protein, sp32, in mammalian sperm is a binding protein specific for two proacrosins and an acrosin intermediate. *J Biol Chem* 269(13): 10133–10140.
15. Ono T, et al. (2001) Identification of proacrosin binding protein sp32 precursor as a human cancer/testis antigen. *Proc Natl Acad Sci USA* 98(6):3282–3287.
16. Tammela J, et al. (2006) OY-TES-1 expression and serum immunoreactivity in epithelial ovarian cancer. *Int J Oncol* 29(4):903–910.
17. Whitehurst AW, et al. (2010) Tumor antigen acrosin binding protein normalizes mitotic spindle function to promote cancer cell proliferation. *Cancer Res* 70(19): 7652–7661.
18. Kanemori Y, et al. (2013) Two functional forms of ACRBP/sp32 are produced by pre-mRNA alternative splicing in the mouse. *Biol Reprod* 88(4):105.
19. Mortimer D, Curtis EF, Miller RG (1987) Specific labelling by peanut agglutinin of the outer acrosomal membrane of the human spermatozoon. *J Reprod Fertil* 81(1): 127–135.
20. Russell LD, Ettlin RA, Sinha Hikim AP, Clegg ED (1990) *Histological and Histopathological Evaluation of the Testis* (Cache River Press, Clearwater, FL).
21. Roqueta-Rivera M, Abbott TL, Sivaguru M, Hess RA, Nakamura MT (2011) Deficiency in the omega-3 fatty acid pathway results in failure of acrosome biogenesis in mice. *Biol Reprod* 85(4):721–732.
22. Ito C, et al. (2013) Integration of the mouse sperm fertilization-related protein equatorin into the acrosome during spermatogenesis as revealed by super-resolution and immunoelectron microscopy. *Cell Tissue Res* 352(3):739–750.
23. Lin YN, Roy A, Yan W, Burns KH, Matzuk MM (2007) Loss of zona pellucida binding proteins in the acrosomal matrix disrupts acrosome biogenesis and sperm morphogenesis. *Mol Cell Biol* 27(19):6794–6805.
24. Fujihara Y, et al. (2012) SPACA1-deficient male mice are infertile with abnormally shaped sperm heads reminiscent of globozoospermia. *Development* 139(19): 3583–3589.
25. Yao R, et al. (2002) Lack of acrosome formation in mice lacking a Golgi protein, GOPC. *Proc Natl Acad Sci USA* 99(17):11211–11216.
26. Shamsadin R, et al. (1999) Male mice deficient for germ-cell cyritestin are infertile. *Biol Reprod* 61(6):1445–1451.
27. Baba D, et al. (2002) Mouse sperm lacking cell surface hyaluronidase PH-20 can pass through the layer of cumulus cells and fertilize the egg. *J Biol Chem* 277(33): 30310–30314.
28. Kim E, et al. (2005) Identification of a hyaluronidase, Hyal5, involved in penetration of mouse sperm through cumulus mass. *Proc Natl Acad Sci USA* 102(50):18028–18033.
29. Honda A, Yamagata K, Sugiura S, Watanabe K, Baba T (2002) A mouse serine protease TESP5 is selectively included into lipid rafts of sperm membrane presumably as a glycosylphosphatidylinositol-anchored protein. *J Biol Chem* 277(19):16976–16984.
30. Miyata H, et al. (2015) Sperm calcineurin inhibition prevents mouse fertility with implications for male contraceptive. *Science* 350(6259):442–445.
31. Matzuk MM, Lamb DJ (2008) The biology of infertility: Research advances and clinical challenges. *Nat Med* 14(11):1197–1213.
32. Perrin A, et al. (2013) Molecular cytogenetic and genetic aspects of globozoospermia: A review. *Andrologia* 45(1):1–9.
33. Dam AHDM, et al. (2007) Homozygous mutation in SPATA16 is associated with male infertility in human globozoospermia. *Am J Hum Genet* 81(4):813–820.
34. Liu G, Shi Q-W, Lu G-X (2010) A newly discovered mutation in PICK1 in a human with globozoospermia. *Asian J Androl* 12(4):556–560.
35. Elinati E, et al. (2012) Globozoospermia is mainly due to DPY19L2 deletion via non-allelic homologous recombination involving two recombination hotspots. *Hum Mol Genet* 21(16):3695–3702.
36. Coutton C, et al. (2012) MLPA and sequence analysis of DPY19L2 reveals point mutations causing globozoospermia. *Hum Reprod* 27(8):2549–2558.
37. Yatsenko AN, et al. (2012) Association of mutations in the zona pellucida binding protein 1 (ZPBP1) gene with abnormal sperm head morphology in infertile men. *Mol Hum Reprod* 18(1):14–21.
38. Zhu F, Gong F, Lin G, Lu G (2013) DPY19L2 gene mutations are a major cause of globozoospermia: Identification of three novel point mutations. *Mol Hum Reprod* 19(6):395–404.
39. Xu X, Toselli PA, Russell LD, Seldin DC (1999) Globozoospermia in mice lacking the casein kinase II alpha′ catalytic subunit. *Nat Genet* 23(1):118–121.
40. Kang-Decker N, Mantchev GT, Juneja SC, McNiven MA, van Deursen JM (2001) Lack of acrosome formation in Hrb-deficient mice. *Science* 294(5546):1531–1533.
41. Yildiz Y, et al. (2006) Mutation of beta-glucosidase 2 causes glycolipid storage disease and impaired male fertility. *J Clin Invest* 116(11):2985–2994.
42. Xiao N, et al. (2009) PICK1 deficiency causes male infertility in mice by disrupting acrosome formation. *J Clin Invest* 119(4):802–812.
43. Lerer-Goldshtein T, et al. (2010) TMF/ARA160: A key regulator of sperm development. *Dev Biol* 348(1):12–21.
44. Paiardi C, Pasini ME, Gioria M, Berruti G (2011) Failure of acrosome formation and globozoospermia in the wobbler mouse, a Vps54 spontaneous recessive mutant. *Spermatogenesis* 1(1):52–62.
45. Audouard C, Christians E (2011) Hsp90β1 knockout targeted to male germline: A mouse model for globozoospermia. *Fertil Steril* 95(4):1475–1477.
46. Pierre V, et al. (2012) Absence of Dpy19l2, a new inner nuclear membrane protein, causes globozoospermia in mice by preventing the anchoring of the acrosome to the nucleus. *Development* 139(16):2955–2965.
47. Wang H, et al. (2014) Atg7 is required for acrosome biogenesis during spermatogenesis in mice. *Cell Res* 24(7):852–869.
48. Tardif S, Guyonnet B, Cormier N, Cornwall GA (2012) Alteration in the processing of the ACRBP/sp32 protein and sperm head/acrosome malformations in proprotein convertase 4 (PCSK4) null mice. *Mol Hum Reprod* 18(6):298–307.
49. Tybulewicz VL, Crawford CE, Jackson PK, Bronson RT, Mulligan RC (1991) Neonatal lethality and lymphopenia in mice with a homozygous disruption of the c-abl proto-oncogene. *Cell* 65(7):1153–1163.
50. Kashiwabara S, et al. (2002) Regulation of spermatogenesis by testis-specific, cytoplasmic poly(A) polymerase TPAP. *Science* 298(5600):1999–2002.
51. Nagai T, Sawano A, Park ES, Miyawaki A (2001) Circularly permuted green fluorescent proteins engineered to sense Ca2+. *Proc Natl Acad Sci USA* 98(6):3197–3202.
52. Okabe M, Ikawa M, Kominami K, Nakanishi T, Nishimune Y (1997) 'Green mice' as a source of ubiquitous green cells. *FEBS Lett* 407(3):313–319.
53. Kashiwabara S, et al. (2000) Identification of a novel isoform of poly(A) polymerase, TPAP, specifically present in the cytoplasm of spermatogenic cells. *Dev Biol* 228(1): 106–115.
54. Yamagata K, Honda A, Kashiwabara SI, Baba T (1999) Difference of acrosomal serine protease system between mouse and other rodent sperm. *Dev Genet* 25(2):115–122.
55. Nishimura H, Kim E, Nakanishi T, Baba T (2004) Possible function of the ADAM1a/ADAM2 Fertilin complex in the appearance of ADAM3 on the sperm surface. *J Biol Chem* 279(33):34957–34962.
56. Toyoda Y, Yokoyama M, Hoshi T (1971) Studies on fertilization of mouse eggs in vitro. *Jpn J Anim Reprod* 16(4):147–151.

57. Yamazaki T, Yamagata K, Baba T (2007) Time-lapse and retrospective analysis of DNA methylation in mouse preimplantation embryos by live cell imaging. *Dev Biol* 304(1): 409–419.
58. Kotaja N, et al. (2004) Preparation, isolation and characterization of stage-specific spermatogenic cells for cellular and molecular analysis. *Nat Methods* 1(3):249–254.
59. Kawano N, et al. (2010) Mice lacking two sperm serine proteases, ACR and PRSS21, are subfertile, but the mutant sperm are infertile in vitro. *Biol Reprod* 83(3):359–369.
60. Mortimer ST (2000) CASA: Practical aspects. *J Androl* 21(4):515–524.
61. Bray C, Son J-H, Kumar P, Meizel S (2005) Mice deficient in CHRNA7, a subunit of the nicotinic acetylcholine receptor, produce sperm with impaired motility. *Biol Reprod* 73(4):807–814.
62. Ogonuki N, et al. (2010) The effect on intracytoplasmic sperm injection outcome of genotype, male germ cell stage and freeze-thawing in mice. *PLoS One* 5(6):e11062.
63. Chatot CL, Ziomek CA, Bavister BD, Lewis JL, Torres I (1989) An improved culture medium supports development of random-bred 1-cell mouse embryos in vitro. *J Reprod Fertil* 86(2):679–688.